The Pressure Gradient Conundrum of Sigma Coordinate Ocean Models

G. L. MELLOR, T. EZER, AND L.-Y. OEY

Program in Atmospheric and Oceanic Sciences, Princeton University, Princeton, New Jersey

(Manuscript received 8 March 1993, in final form 8 November 1993)

ABSTRACT

Much has been written of the error in computing the horizontal pressure gradient associated with sigma coordinates in ocean or atmospheric numerical models. There also exists the concept of "hydrostatic inconsistency" whereby, for a given horizontal resolution, increasing the vertical resolution may not be numerically convergent.

In this paper, it is shown that the differencing scheme cited here, though conventional, is not hydrostatically inconsistent; the sigma coordinate, pressure gradient error decreases with the square of the vertical and horizontal grid size. Furthermore, it is shown that the pressure gradient error is advectively eliminated after a long time integration. At the other extreme, it is shown that diagnostic calculations of the North Atlantic Ocean using rather coarse resolution, and where the temperature and salinity and the pressure gradient error are held constant, do not exhibit significant differences when compared to a calculation where horizontal pressure gradients are computed on z-level coordinates. Finally, a way of canceling the error ab initio is suggested.

1. Introduction

The use of sigma coordinates, wherein the water column is divided into the same number of grid cells independent of depth, is attractive when dealing with bottom topography. It has been seen that estuaries are modeled rather well (Oey et al. 1985a,b; Galperin and Mellor 1990a,b); one needs to model the bottom boundary layer to correctly represent tidal mixing. Evidence is accumulating that sigma coordinates can accommodate rather sharp topographical changes that include a continental shelf with an adjacent shelf break and deep ocean (Haidvogel et al. 1991; Ezer and Mellor 1992) and seamounts (Ezer 1994).

However, recent papers by Haney (1991) and others have evoked concern in the ocean modeling community that the use of sigma coordinates may cause significant errors when dealing with steep topography. We mostly defer to Haney's introduction, which nicely provides historical background emanating from the meteorological literature but we will briefly repeat some salient points. He notes, for example, that Rousseau and Pham (1971), Janjic (1977), and Mesinger (1982) have identified the related problem of "hydrostatic consistency" corresponding to

$$\left|\frac{\sigma}{H}\frac{\delta_x H}{\delta\sigma}\right| < 1, \tag{1}$$

where σ is the vertical sigma coordinate, defined below; H is the depth; $\delta_x H$ is the horizontal change in depth of adjacent grid cells; and $\delta\sigma$ is the vertical cell size associated with a sigma grid cell, $\delta x \delta\sigma$. If (1) is not satisfied, the finite-difference scheme is purportedly nonconvergent. Haney concludes that "It is obviously essential to choose the horizontal and vertical resolution carefully, not only to accommodate the particular ocean problem at hand, but also to satisfy the hydrostatic consistency condition" [see Eq. (1)]. However, adherence to (1) would be severely restrictive. For example, with 20 evenly spaced sigma levels, (1) leads to the constraint, $\delta_x H/H < 0.05$. With present computing resources, one would have to smooth bottom topography in, say, a basin-scale model to the extent that it may no longer resemble the basin. Equation (1) would also mitigate against the use of a refined σ grid near the bottom to better resolve the bottom boundary layer (where $\sigma = -1$; a similar problem does not exist in the surface layer where $\sigma = 0$).

2. The pressure gradient error

We restrict attention to two dimensions until section 4. Let (x^*, z) denote Cartesian coordinates and (x, σ) sigma coordinates. Although the relationship between (x^*, z) and (x, σ) may be generalized (Gerdes 1993), we cite here the specific and conventional relationship

$$x^* = x, \tag{2a}$$

$$z = \sigma H(x), \tag{2b}$$

where z and σ increase vertically upward such that $z = \sigma = 0$ at the surface and $\sigma = -1$ and $z = -H$ at the bottom.

Corresponding author address: Dr. George L. Mellor, Program in Atmospheric and Oceanic Sciences, Princeton University, P.O. Box CN710, Sayre Hall, Princeton, NJ 08544-0710.
E-mail: glm@splash.princeton.edu

© 1994 American Meteorological Society

The kinematic pressure (pressure divided by a reference density) will be denoted by p. The horizontal gradient of pressure, $p^* = p^*(x^*, z)$ in Cartesian coordinates, when evaluated from the pressure, $p = p(x, \sigma)$, in sigma coordinates is

$$\frac{\partial p^*}{\partial x^*} = \frac{\partial p_0}{\partial x} + H \int_\sigma^0 \frac{\partial b^{*\prime}}{\partial x^*} d\sigma', \tag{3a}$$

where $b^{*\prime} = b^*(x^*, \sigma')$ and

$$\frac{\partial b^*}{\partial x^*} = \frac{\partial b}{\partial x} - \frac{\sigma}{H}\frac{\partial H}{\partial x}\frac{\partial b}{\partial \sigma}. \tag{3b}$$

The buoyancy is $b = \rho g/\rho_0$ where ρ is the density; ρ_0 is a constant reference density; g is the gravity constant; $H = H(x)$ is the bottom topography; and $p_0 = p_0(x)$.

Alternatively, the pressure gradient may be written

$$\frac{\partial p^*}{\partial x^*} = \frac{\partial p}{\partial x} - \frac{\sigma}{H}\frac{\partial H}{\partial x}\frac{\partial p}{\partial \sigma}, \tag{4a}$$

where

$$p(x, \sigma) = p_0(x) + H \int_\sigma^0 b' d\sigma'. \tag{4b}$$

Equations (3a) and (3b) and (4a) and (4b) are equivalent analytically. However, they may differ after approximation by finite difference algebra.

The model used here (Blumberg and Mellor 1987; Mellor 1992) invokes (3a) and (3b) to obtain the horizontal pressure gradient. [Our model has a free surface so that p_0, the surface pressure, is given by $p_0 = b(x, 0)\eta(x)$, where η is the surface elevation and H should be replaced by $H + \eta$ in (3a) and (3b). However, the discussion of the main issue of this paper is somewhat simpler in terms of a rigid-lid model. Results are easily generalized to a free surface model. The calculations cited below will be executed by our free surface model.] Haney (1991) and others use the finite difference analog of (4a) and (4b).

When initializing a sigma coordinate model, the procedure usually is to interpolate data, $b(z)$, at a given horizontal location, $x^* = x$, to $b(\sigma)$; we use a cubic-spline interpolation (Press et al. 1986). Then one finds that the finite-difference reckoning of $\partial b^*/\partial x^*$ of the original dataset does not equal that determined in the sigma system because each of the two terms on the right sides of (3b) or (4a) are generally much larger than their difference. This can be most easily seen in the case of a field where $b^* = b^*(z)$ and $\partial b^*/\partial x^* = 0$; the two terms on the right side of (3b) should cancel and do so analytically. However, the finite-difference representation of the terms contain truncation errors and a net truncation error is introduced.

One way (Gary 1973) to counteract the error is to calculate an area-averaged $b_0^*(z) \equiv \langle b^*(x, z)\rangle$, interpolate that field onto the sigma field, and then subtract it from $b(x, \sigma)$ before executing the finite-difference form of (3b). In the case where $b^* = b^*(z)$, the error is totally eliminated. In the case where $b^* = b(x, z)$, much of the error is eliminated. This has been our standard practice for regional models and does eliminate much of the truncation error. However, for basin-scale or global models, where vertical variability will depart significantly from the area mean, it remains to be shown whether or not the remaining error is significant.

A finite-difference scheme and error evaluation. If we refer to the computational stencil in Fig. 1, we find that (3b) may be written

$$\frac{\delta_x b^*}{\delta x^*} = \frac{b_{i,k} + b_{i,k-1} - b_{i-1,k} - b_{i-1,k-1}}{2\delta x} - \frac{\bar{\sigma}\delta_x H}{\bar{H}\delta x}\frac{b_{i,k-1} + b_{i-1,k-1} - b_{i,k} - b_{i-1,k}}{2\delta\sigma}, \tag{5}$$

where $\bar{\sigma} = (\sigma_{k-1} + \sigma_k)/2$, $\bar{H} = (H_i + H_{i-1})/2$, $\delta x = x_i - x_{i-1}$, $\delta\sigma = \sigma_{k-1} - \sigma_k$, and $\delta_x H = H_i - H_{i-1}$.

The error can be made most transparent by a "data" field such that $b^* = b^*(z)$, where one should obtain $\delta_x b^*/\delta x^* = 0$. However, if we expand $b(x, \sigma)$ around some point, $z_0 = \bar{\sigma}\bar{H}$, such that, in sigma coordinates,

$$b^*(z) = b_0 + \left(\frac{\partial b}{\partial z}\right)_0 [\sigma H(x) - z_0] + \left(\frac{\partial^2 b}{\partial z^2}\right)_0 \frac{[\sigma H(x) - z_0]^2}{2} + \cdots \tag{6}$$

and insert (6) into (5), we obtain the incremental error for finite $\delta\sigma$ and δH,

$$E\left(\frac{\delta_x b^*}{\delta x^*}\right) = \frac{H}{4}\frac{\delta_x H}{\delta x}\left[\left(\frac{\partial^2 b}{\partial z^2}\right) + \frac{\sigma H}{3}\left(\frac{\partial^3 b}{\partial z^3}\right) + \cdots\right] \times \left\{(\delta\sigma)^2 - \sigma^2\left(\frac{\delta_x H}{H}\right)^2\right\}. \tag{7}$$

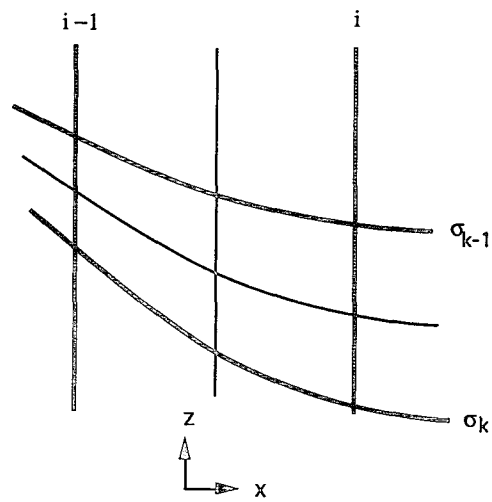

FIG. 1. The computational stencil for Eq. (5).

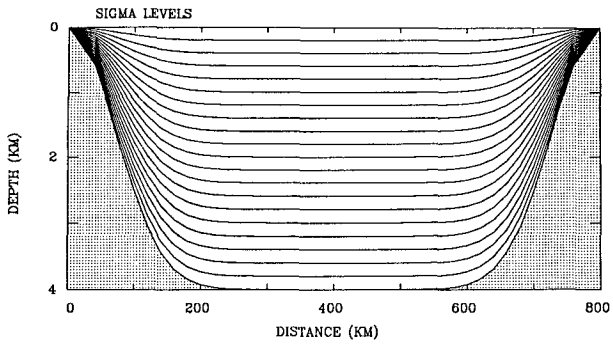

FIG. 2. The test basin showing contours of constant σ that range from -1 (the bottom) to 0 (the surface). The horizontal grid interval is 20 km.

We have removed the overbars on σ and H and the subscripts, 0, and note that all terms should now be subscripted with appropriate i's and k's. The total error will be the incremental error according to (7), summed according to the finite-difference form of (3a).

Note that the error is null for linear profiles of b as may be obtained directly from (5) for $b \propto \sigma H(x)$.

Since there is a negative sign in the right side of (7), one obtains zero incremental error when $|(\sigma\delta_x H)/(H\delta\sigma)| = 1$, the condition where σ at $i - 1$ (or i) corresponds to the same value of z for $\sigma + \delta\sigma$ at i (or $i - 1$). The condition, $|(\sigma\delta_x H)/(H\delta\sigma)| > 1$, is said to represent a "hydrostatically inconsistent" grid since, for fixed $|\delta_x H/H|$, the error increases for decreasing $|\delta\sigma/\sigma|$. However, the negative sign in (7) generally reduces error and is therefore a fortuitous circumstance. In any event, the error does decrease as $\delta\sigma \to 0$ and $\delta H \to 0$ (or, equivalently, $\delta x \to 0$). In fact it would seem to be a conceptual error to factor out $\delta\sigma^2$ from the term in curly brackets to obtain $\delta\sigma^2\{1 - (\sigma^2\delta_x H^2)/(H^2\delta\sigma^2)\}$ and then base discussion on the factor, $|(\sigma\delta_x H)/(H\delta\sigma)|$. For example, that factor, unto itself, might lead one to believe that a choice of small $\delta\sigma$'s near the bottom to resolve bottom boundary layers might be numerically hazardous. Previously, we had not perceived this to be the case during the course of a detailed study of the bottom boundary layer (Mellor 1986); now, Eq. (7) corroborates that perception.

We have repeated the above analysis for (4a) and (4b) which first can be written

$$\frac{\partial p^*}{\partial x^*} = \frac{\partial p_0}{\partial x} + \int_\sigma^0 \left[\frac{\partial b' H}{\partial x} - \frac{\partial H}{\partial x}\frac{\partial \sigma' b'}{\partial \sigma'}\right] d\sigma'.$$

The error in the integrand can be evaluated as before and, somewhat to our surprise, the error is also given by (7).

3. The error appears and disappears

A two-dimensional version of our model is applied here to the basin and grid depicted in Fig. 2. It is initialized with the potential density,

$$\frac{\rho}{\rho_0} = 1.028 - 0.003 \exp\left(\frac{z}{1000 \text{ m}}\right),$$

which is a close approximation to the area-averaged, vertical distribution for the North Atlantic Ocean (Levitus 1982). Importantly, there are no horizontal density gradients in (x^*, z) coordinates. Model calculations will use a constant horizontal viscosity of 2000 m^2 s^{-1} and a vertical viscosity of 10^{-3} m^2 s^{-1} (a value of zero yields essentially the same results as those discussed below). The Coriolis parameter is 10^{-4} s^{-1}. There are 21 sigma levels with a constant spacing of $\delta\sigma = 0.05$. There are 41 grid nodes in the x direction with a spacing of $\delta x = 20$ km. The maximum values of $|(\delta_x H)/H|$ and $|(\sigma\delta_x H)/H\delta\sigma)|$ are about 0.67 and 13, respectively. There is no surface forcing and the vertical and horizontal diffusivities are null. It is only under these circumstances that an exact solution, null velocities and no change in density, is known.

a. A diagnostic calculation

We first run the model diagnostically (density is fixed) for 90 days. The spatially averaged kinetic energy and potential energy is shown in Fig. 3. The truncation error drives the model such that the maximum kinetic energy ($\approx$5 cm^2 s^{-2}) is obtained after one day; there are barotropic waves in evidence and these decay due to horizontal viscosity such that they have nearly vanished by day 90. In Fig. 4 we display the alongshore velocities after 90 days. The fields are antisymmetric about $x = 400$ km. These are the (nearly geostrophic) velocity errors due to the errors in the calculation of $\delta_x b^*/\delta x^*$; the maximum error is about 7 cm s^{-1}. The error in the vertically averaged velocity is about 1.5 cm s^{-1}.

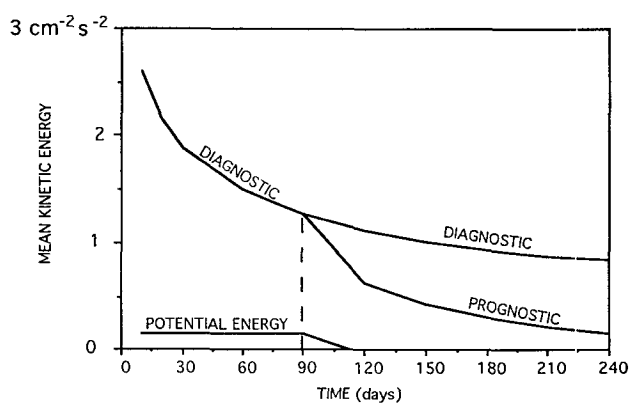

FIG. 3. The spatially averaged kinetic energy (cm^2 s^{-2}) as a function of time. The model is run diagnostically (density held constant) for 90 days and thereafter prognostically; the mean kinetic energy asymptotes to zero. (Continuation of the diagnostic run is also shown; it asymptotes to 0.70 cm^2 s^{-2}.) The mean potential energy relative to that at day 720 is also shown in the same units as the kinetic energy.

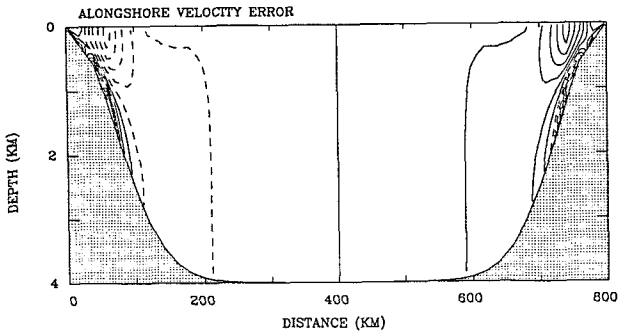

FIG. 4. The alongshore velocity field after the model has run diagnostically for 90 days. The contour interval is 0.1 cm s^{-1}. The largest velocities are ±5 cm s^{-1} near the surface and ±7 cm s^{-1} near the 1000-m isobath. After running prognostically for a subsequent two years, the velocities have decreased by almost two orders of magnitude; they decrease indefinitely with further run time.

The model has also been run with the resolution refined by a factor of 2. The change in $\delta\sigma$ has little effect but the error due to the change in δx and, therefore, $\delta_x H$ reduces the error by a factor of 4. All of this is in compliance with (7).

b. Prognostic continuation

After day 90, the density field is allowed to advect in the (x, σ) plane; the velocity field dissipates and the mean kinetic energy and potential energy decrease. After day 720, the maximum error is 0.2 cm s^{-1}; the error continues to decrease with additional run time.

The velocity field has spun down under the control of viscosity while at the same time the density field has advectively adjusted so as to cancel out the false baroclinicity due to the sigma coordinate truncation error. In the appendix, the spindown problem is formulated as a linear, low–Rossby number problem wherein velocity advection is neglected and where buoyancy advection is replaced by wN^2; w is the vertical velocity and $N(z)$ is the Brunt–Väisälä frequency. The process is analogous to the spindown of oceanic rings (Flierl and Mied 1985). In any event, the density field has relaxed to a new field such that $\delta_x b^*/\delta x^* = 0$, as evaluated according to (5). The new field, plotted in (x^*, z) coordinates, would not exhibit a discernible difference compared to the original density field. In Fig. 5a we show the change in the density field in sigma-θ units.

Now, the other quantity needed by some models is the vertical stability that is used in turbulence parameterization for vertical mixing (Munk and Anderson 1948; Mellor and Yamada 1982; Pacanowski and Philander 1981) and that also factors into the Rossby radius of deformation. In Fig. 5b we plot the change in the Brunt–Väisälä frequency squared, which can be used to calculate a Richardson number or the Rossby radius, and we obtain values of about 6% in the shallowest water and near the bottom; smaller values prevail elsewhere. This is not a physically significant change.

What we have learned from the simple test problem is that the system of interpolating to the σ coordinate grid, with subsequent use of transformations such as (3a) and (3b), will produce errors in the velocity field (and surface elevation), but upon model prognostic execution, these velocity errors are eliminated from the final equilibrium fields; density errors are created, however. The density errors can be evaluated in terms of vertical density gradients and these errors do seem rather inconsequential.

We believe, but cannot prove, that the "advective error elimination" process should prevail in the general case with surface forcing and with diffusivities. Variations in $b(x, y, \sigma, t)$ due to surface buoyancy flux or through dynamical adjustment to surface wind stress are likely to be surface trapped and to be small relative to initial errors. The newly evolved $b(x, y, \sigma, t)$, constituting new initial conditions, should also be advectively eliminated. However, to the best of our knowledge, ways of quantitatively evaluating errors for more general cases are not known.

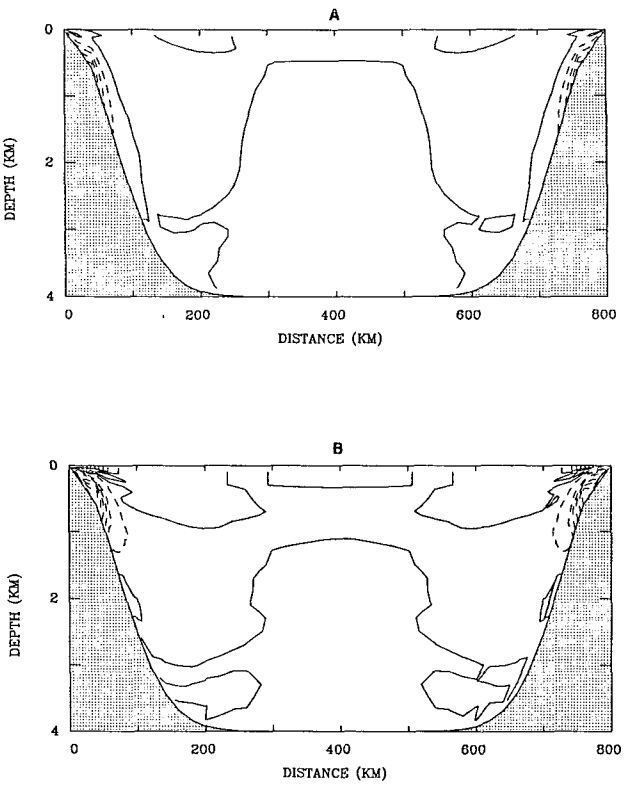

FIG. 5. (a) The density field change in sigma-θ units between day 720 and day 0; the contour interval is 0.01 and the largest change is a negative 0.07. (b) The percentage change in the Brunt–Väisälä frequency squared between day 720 and day 0; the contour interval is 1% and the largest change is a negative 6%. The solid lines are zero contours.

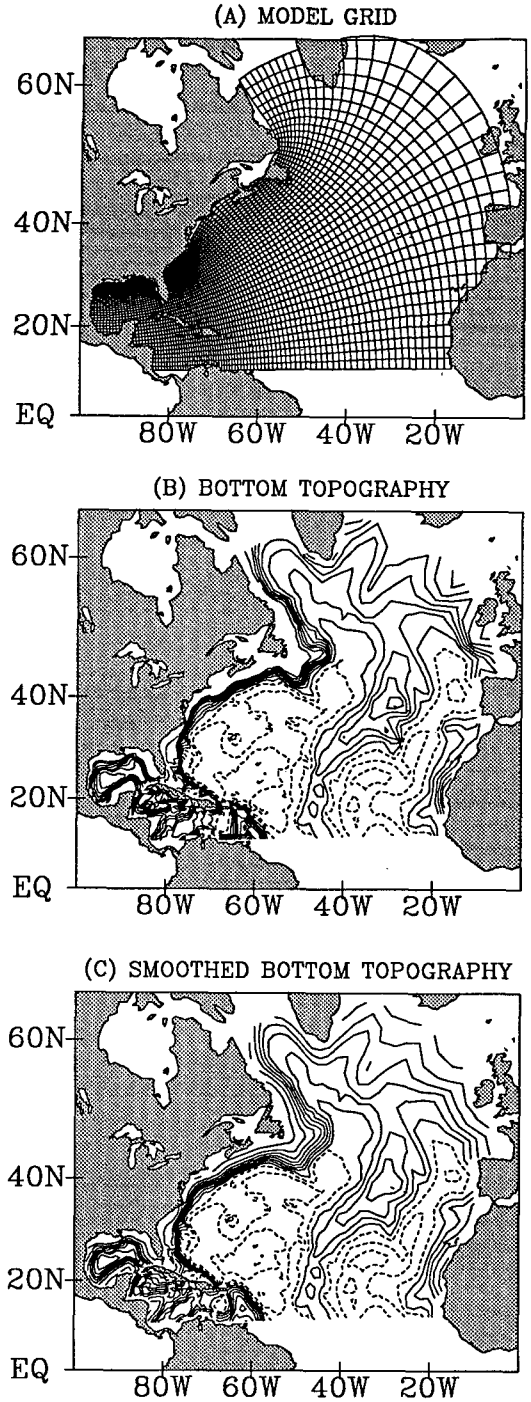

FIG. 6. (a) The North Atlantic model grid. (b) The bottom topography. (c) The bottom topography after smoothing such that $\delta H/H \leq 0.4$. The contour interval in (b) and (c) is 500 m; dashed contours indicate $H > 4000$ m.

The above results suggest that a way of coping with the sigma coordinate error is to simply run the model to a statistically stationary (but not necessarily steady) equilibrium, the solution depending on the surface and lateral boundary conditions. This strategy should apply in the case of climate modeling and any application where run time is longer than diffusion time scales. For short model runs, we propose another way to defeat the problem in section 5, based on experience gained in the next section.

4. Three-dimensional diagnostic calculations

Suppose one does not wish to run the model to equilibrium. One may have in hand a climatology that is believed to be correct at least for the larger scales. One may wish to obtain the velocity fields associated with the climatology.

At the moment we are working on a model of the North Atlantic; we use this as a test bed to investigate the pressure gradient error in a more or less real application. Here, it serves our purpose to run the model diagnostically; that is, the model temperatures and salinities are fixed at the values obtained by Levitus (1982), which are interpolated onto the model grid. An equation of state (Mellor 1991) provides density as a function of potential temperature and salinity. The orthogonal, curvilinear, model grid and two bathymetries are shown in Fig. 6. The grid element size is variable such that in the Gulf Stream and the Gulf of Mexico the elements are 30–50 km, whereas in the northeast Atlantic they are as large as 200 km. We will refer both to the standard Levitus z-level grid (33 levels with 10-m intervals near the surface and 500-m intervals below a depth of 2000 m) and the sigma grid (15 sigma levels with smallest $\delta\sigma = 0.002$ near the surface and $\delta\sigma = 0.125$ below $\sigma = -0.125$). With this coarse resolution we believe that results are improved with some topographical smoothing. With an eye on (7), the topography at two adjacent grid elements are mutually adjusted, so that $|\delta H/H| \leq \mathrm{SF}$ (where SF is a slope factor that ranges from 0 to 2.0, the maximum theoretical value) while conserving the total water column volume of the two grid elements. The grid is then repeatedly scanned in alternating directions until there are no further changes. Note that most topographical values are unaffected with say a value of SF = 0.4. For example an adjacent gridpoint change in depth from 1000 to 1500 m would, per se, not be altered. However, we do add a further five-point Laplacian smoother; this filter is mainly cosmetic although in the poorly resolved northwestern part of the model, it does add further noticeable smoothing.

Figure 6b is the topography interpolated from the Navy's DBDB5 $1/12° \times 1/12°$ bathymetric file after the Laplacian filter, but without slope adjustment (SF = 2.0; a maximum value of $|\delta H/H| \approx 1$ is obtained), whereas for Fig. 6c the value SF = 0.4 is stipulated. (The maximum slope, $\delta H/\delta y \approx 0.05$, is obtained at the Puerto Rican Trench before and after slope adjustment.) Note that, except for some widening of the continental slope, most of the topographic features of the basin are unaffected by the smoothing procedure.

Another type of diagnostic calculation by Mellor et al. (1982), repeated and extended by Greatbatch et al. (1991), shows that the total transport (vertically integrated velocity) normal to the zonal transect at 10°N is approximately null. For the limited basin used here, we have set to zero the total transport normal to 10°N and also on the northern boundaries where the total transport is known to be small. As detailed, for example, by Ezer and Mellor (1992), the vertical distributions of horizontal velocities are governed by geostrophy on the open boundaries and the normal components integrate to zero. The model is driven by annually averaged climatological winds, obtained from the Comprehensive Ocean–Atmosphere Data Set analyzed by Wright (1988); a detailed description of the surface forcing formulation in the model can be found in Ezer and Mellor (1992).

The following three types of calculation were performed:

(I) The horizontal density gradients are evaluated on the curvilinear horizontal grid but with the standard z-level depths. The vertical integration in (3a) is also carried out on the same grid. Then the gradients are interpolated to the sigma grid; they are, of course, held constant during the diagnostic calculation. The pressure gradient truncation error is null in this case.

(II) Our standard "sigma" calculation with no corrections. Thus, we first interpolate temperature and salinity from the horizontal $1° \times 1°$ Levitus grid with standard z-level depths onto the horizontal curvilinear grid but with the same standard z levels. Next, with reference to Fig. 7, the temperatures and salinities are interpolated to the sigma grid and the equation of state provides densities. The baroclinic density gradients are calculated according to (5) on the sigma grid and then integrated according to the finite-difference analog of (3a).

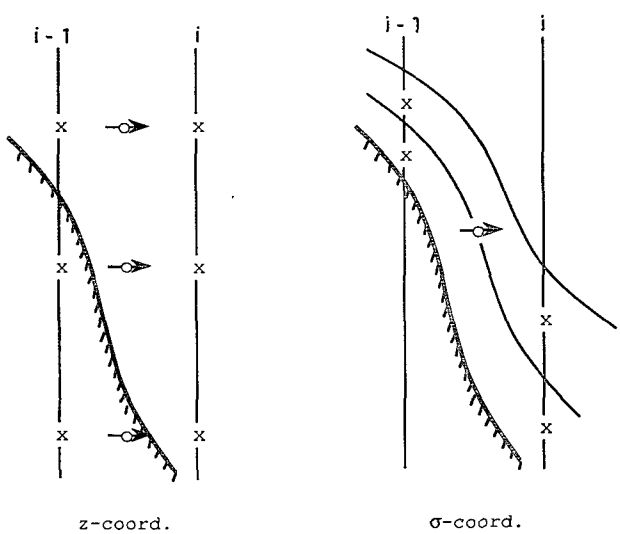

FIG. 7. The left-hand side of the diagram depicts a z-level coordinate system on the horizontal curvilinear grid. The right side depicts a sigma coordinate system. Temperatures, salinities, or densities are denoted by the crosses; density gradients are denoted by the open circle and arrow.

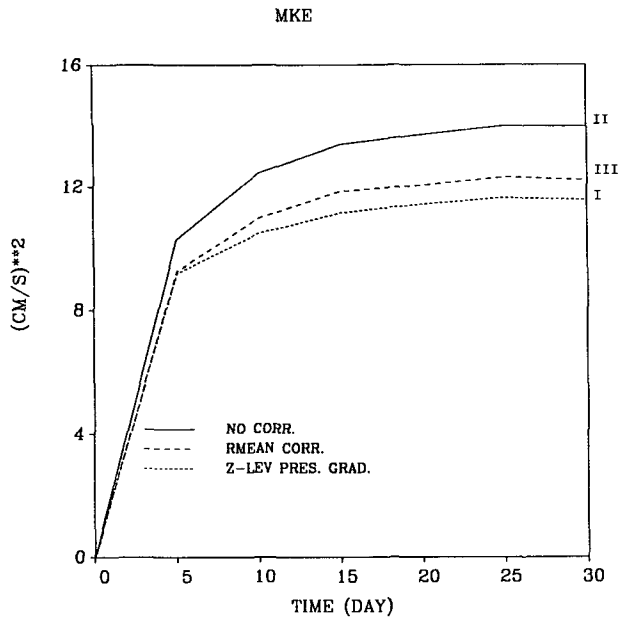

FIG. 8. The volume-averaged mean kinetic energy from the three-dimensional diagnostic calculations. The pressure gradient forcing is calculated: I—with density gradients evaluated on the z levels (dotted line); II—with the standard sigma-level formulation (solid line); and III—with the standard sigma-level formulation but where the area mean density field is first subtracted (dashed line).

(III) The same as case II except that the area-averaged density is first subtracted before the right side of (5) is evaluated. Note that $\rho = \rho_1(\Theta, S) + \rho_2(\Theta, S, p)$; we use the UNESCO equation of state as modified by Mellor (1991). The second, pressure-dependent part is weakly dependent on potential temperature Θ and salinity S. Subtracting the area average $\bar{\rho}(z)$ eliminates almost all of the error associated with the second term and some of the error associated with the first term.

It should be noted that, while the pressure gradient truncation error, as we have defined it, is null in case I, there is an error associated with the fact that, as illustrated in Fig. 7, there are points at, say, i that are adjacent to points at $i - 1$, which are under the bottom. In these cases we have set the gradient to zero. A presumably more rational interpolation scheme would lead us back to (5). A recent paper by Gerdes (1993) deals with a comparison of sigma coordinate and z-level models and indicates that errors associated with the latter are more pronounced than those of the former.

The diagnostic calculation is run for 30 days and the volume-averaged kinetic energies are shown in Fig.

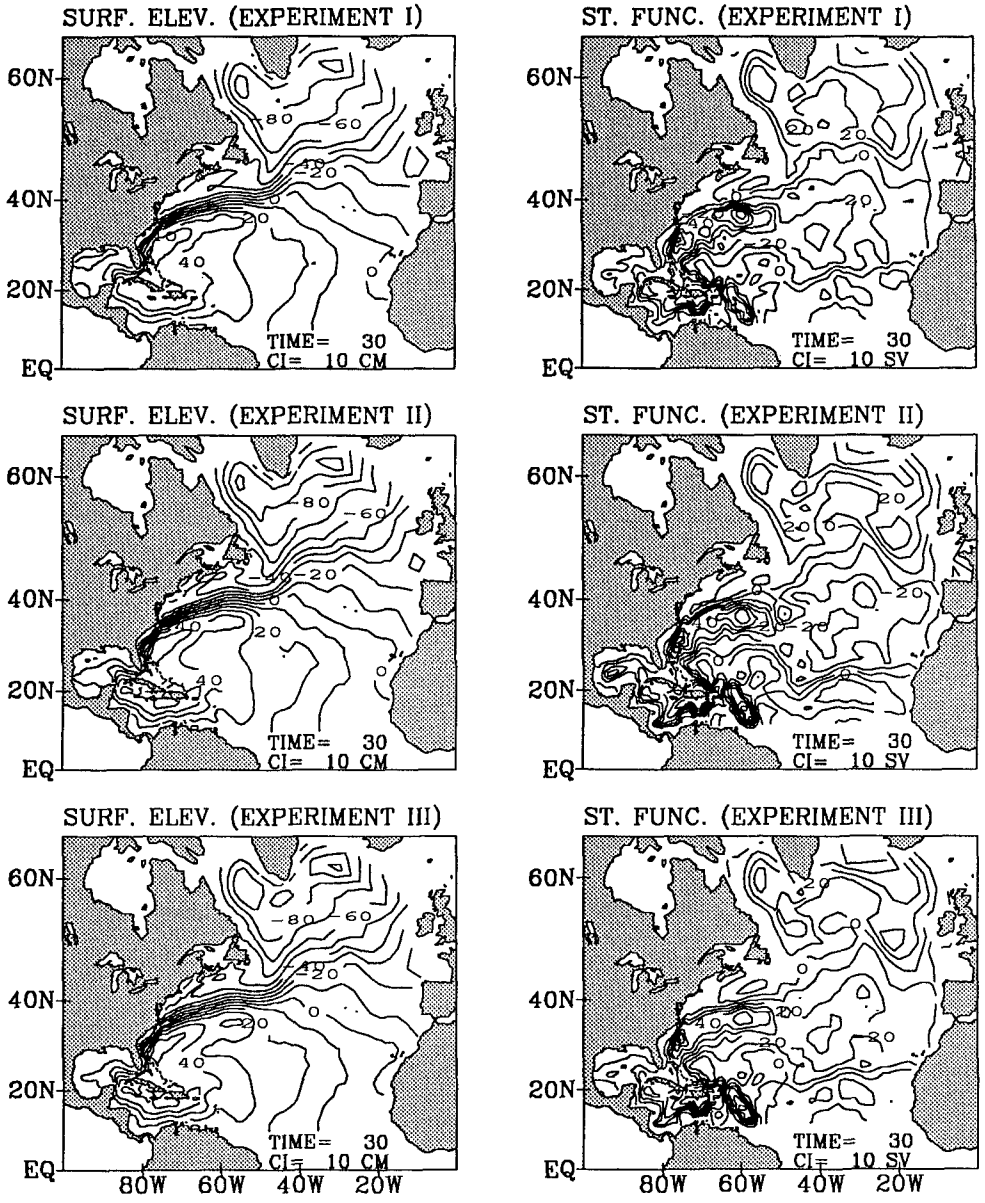

FIG. 9. The surface elevation (left panels) and the total streamfunction (right panels): for case I, where density gradients are calculated on the z-level grid; case II, where they are evaluated on the sigma grid; and case III, which is the same as II except that the area mean density is first subtracted before calculation of the density gradients.

8 for the three cases. (Note that equilibrium is achieved faster in the three-dimensional calculation compared to the two-dimensional calculation; presumably barotropic waves can disburse more readily in the former case.) The total streamfunction, indicative of the deeper velocities, and the surface elevation whose gradients represent the surface geostrophic velocity are plotted in Fig. 9 for the three cases.

It is somewhat surprising to us that there are so few differences in the three cases but that is our finding. In particular, there is almost no difference in surface elevation. There are differences in the total streamfunction between cases I and II, particularly in the Gulf of Mexico; however, this difference is reduced significantly by the correction used in case III. Note that the resolution is quite crude here relative to emerging computer capabilities. Improved vertical and horizontal resolution should further narrow the differences. In particular, recall that the sigma coordinate, pressure gradient error, which now seems rather benign, goes as the square of horizontal and vertical increments according to (7).

5. Conclusions

We conclude the following:

1) The sigma coordinate, pressure gradient error is not numerically divergent; the error decreases as the square of both the vertical and horizontal grid element size. More generally, (7) provides a tool to evaluate the error.

2) There is evidence presented here that initial pressure gradient errors in dynamic variables will be advectively eliminated. There will be created small compensatory errors in the density (and temperature and salinity) field.

3) An evaluation of initial pressure gradient errors in the case of a relatively crude resolution Atlantic Ocean model indicates that the errors should not cause serious concern. The errors are reduced by subtraction of the area-averaged density gradient before evaluation of the density gradient on the sigma coordinate grid.

We finally note that the procedure developed in section 4, where the density gradient is first evaluated on the z-level grid, suggests a simple way of correcting the initial sigma error. We write (3b) as

$$\frac{\partial b^*}{\partial x^*} = \frac{\partial b}{\partial x} - \frac{\sigma}{H}\frac{\partial H}{\partial x}\frac{\partial b}{\partial \sigma} + \epsilon_x(x, \sigma).$$

Evaluate the left side on the standard z-level grid, and the first two terms on the right on the sigma grid; then evaluate $\epsilon_x(x, \sigma)$. During all subsequent calculations on the sigma grid, diagnostic or prognostic, $\epsilon_x(x, \sigma)$ is held constant. In this way "the pressure gradient error" is canceled. This procedure works in the case of section 4 wherein the initial velocity field is null and renders cases II and III identical to case I in section 4. A related idea has previously been proposed by Sundqvist (1976).

APPENDIX

The Velocity Error Removal Process

It is useful to reduce the process of density error cancellation and velocity error removal to the simplest relevant system.

Let (u, v, w) and b be the velocity and buoyancy that evolve as a result of an initial pressure gradient truncation error $\epsilon(x, z)$. The relevant linear problem is (exclusive of appropriate boundary and initial conditions):

$$\frac{\partial u}{\partial x} + \frac{\partial w}{\partial z} = 0, \tag{A1}$$

$$-f\frac{\partial v}{\partial z} = \frac{\partial b}{\partial x} + \epsilon(x, z), \tag{A2}$$

$$\frac{\partial v}{\partial t} + fu = A\frac{\partial^2 v}{\partial x^2}, \tag{A3}$$

$$\frac{\partial b}{\partial t} - N^2 w = 0. \tag{A4}$$

At $t = 0$, $u = w = b = 0$ and $\partial v/\partial z = -f^{-1}\epsilon(x, z)$. It can then be shown that the system decays to the asymptotic state, $u = v = w = \partial b/\partial t = 0$ and $\partial b/\partial x = -\epsilon(x, z)$. For a horizontal scale of 100 km appropriate to the topographic scale in Fig. 2 and $A = 2000$ $m^2\ s^{-1}$, we obtain a viscous decay timescale of about 60 days, which is approximately the decay time in Fig. 3 as the calculation switches from diagnostic to prognostic. Figure 3 also shows a longer decay scale corresponding to barotropic wave decay (see the curve labeled "diagnostic"); for the appropriate scale of one-half basin width, we obtain a timescale of about 1000 days for that irrelevant process.

Note that the advection term, $N^2 w$ in (A4), is crucial to the above adjustment process, and so we have used the term "advectively eliminated" to describe the process of density gradient error cancellation and velocity error removal.

Acknowledgments. The study has been supported by the Navy Ocean Modeling and Prediction Program of the Office of Naval Research, the National Ocean Service (through the NJ Sea Grant Program), and NOAA's Geophysical Fluid Dynamics Laboratory. Prof. R. L. Haney contributed valuable comments.

REFERENCES

Blumberg, A. F., and G. L. Mellor, 1987: A description of a three-dimensional coastal ocean circulation model. *Three-Dimensional Coastal Ocean Models,* Vol. 4, N. Heaps, Ed., American Geophysical Union, 208 pp.

Ezer, T., 1994: On the interaction between the Gulf Stream and the New England seamount chain. *J. Phys. Oceanogr.,* **24,** 191–204.

——, and G. L. Mellor, 1992: A numerical study of the variability and the separation of the Gulf Stream induced by surface atmospheric forcing and lateral boundary flows. *J. Phys. Oceanogr.,* **22,** 660–682.

Flierl, G. F., and R. P. Mied, 1985: Frictionally induced circulations and spin down of a warm-core ring. *J. Geophys. Res.,* **90,** 8917–8927.

Galperin, B., and G. L. Mellor, 1990a: A time-dependent, three-dimensional model of the Delaware Bay and River. Part 1: Description of the model and tidal analysis. *Estuarine, Coastal Shelf Sci.,* **31,** 231–253.

——, and ——, 1990b: A time-dependent, three-dimensional model of the Delaware Bay and River. Part 2: Three-dimensional flow fields and residual circulation. *Estuarine, Coastal Shelf Sci.,* **31,** 255–281.

Gary, J. M., 1973: Estimate of truncation error in transformed coordinate, primitive equation atmospheric models. *J. Atmos. Sci.,* **30,** 223–233.

Gerdes, R., 1993: A primitive equation model using a general vertical coordinate transformation 1. Description and testing of the model. *J. Geophys. Res.,* **98,** 14 683–14 701.

Greatbatch, R. J., A. F. Fanning, A. D. Goulding, and S. Levitus, 1991: A diagnosis of interpentadal circulation changes in the North Atlantic. *J. Geophys. Res.,* **96,** 22 009–22 023.

Haidvogel, D. B., A. Beckman, and K. S. Hedstrom, 1991: Dynamical simulations of filament formation and evolution in the coastal transition zone. *J. Geophys. Res.,* **96,** 15 017–15 040.

Haney, R. L., 1991: On the pressure gradient force over steep topography in sigma coordinate ocean models. *J. Phys. Oceanogr.,* **21,** 610–619.

Janjic, Z. I., 1977: Pressure gradient force and advection scheme used for forecasting with steep and small scale topography. *Contrib. Atmos. Phys.*, **50**, 186–199.

Levitus, S., 1982: *Climatological Atlas of the World Ocean.* U.S. Dept. of Commerce and NOAA, 173 pp.

Mellor, G. L., 1986: Numerical simulation and analysis of the mean coastal circulation off California. *Contin. Shelf Res.*, **6**, 689–713.

——, 1991: An equation of state for numerical models of ocean and estuaries. *J. Atmos. Oceanic Technol.*, **8**, 609–611.

——, 1992: User's guide for a three-dimensional, primitive equation, numerical ocean model. Program in Atmospheric and Oceanic Sciences, Princeton University, Princeton, NJ, 35 pp.

——, and T. Yamada, 1982: Development of a turbulence closure model for geophysical fluid problems. *Rev. Geophys. Space Phys.*, **20**, 851–875.

——, C. Mechoso, and E. Keto, 1982: A diagnostic calculation of the general circulation of the Atlantic Ocean. *Deep-Sea Res.*, **29**, 1171–1192.

Mesinger, F., 1982: On the convergence and error problems of the calculation of the pressure gradient force in sigma coordinate models. *Geophys. Astrophys. Fluid Dyn.*, **19**, 105–117.

Munk, W. H., and E. R. Anderson, 1948: Notes on a theory of the thermocline. *J. Mar. Res.*, **7**, 276–295.

Oey, L.-Y., G. L. Mellor, and R. I. Hires, 1985a: A three-dimensional simulation of the Hudson–Raritan estuary. Part I: Description of the model and model simulations. *J. Phys. Oceanogr.*, **15**, 1676–1692.

——, ——, and ——, 1985b: A three-dimensional simulation of the Hudson–Raritan estuary. Part II: Comparison with observation. *J. Phys. Oceanogr.*, **15**, 1693–1709.

Pacanowski, R. C., and S. G. H. Philander, 1981: Parameterization of vertical mixing in numerical models of tropical oceans. *J. Phys. Oceanogr.*, **11**, 1443–1451.

Press, W. H., B. P. Flannery, S. A. Teukolsky, and W. T. Vetterling, 1986: *Numerical Recipes, The Art of Scientific Computing.* Cambridge University Press, 818 pp.

Rousseau, D., and H. L. Pham, 1971: Premiers resultat d'un modele de prevision numerique a courte echeance sur l'Europe. *La Meteorologie*, **20**, 1–12.

Sundqvist, H., 1976: On vertical interpolation and truncation in connection with use of sigma system models. *Atmosphere*, **14**, 37–52.

Wright, P. B., 1988: An atlas based on the COADS data set: Fields of mean wind, cloudiness and humidity at the surface of the global ocean. Max-Planck Institüt für Meteorologie Report No. 14, Hamburg, Germany, 68 pp.